環境流体における移流拡散反応現象の数理モデリングと環境科学への応用

研究代表者　研　究　員　**大春慎之助**（中央大学理工学部）
共同研究者　研　究　員　**杉山　高一**（中央大学理工学部）
共同研究者　研　究　員　**松下　貢**（中央大学理工学部）
共同研究者　研　究　員　**山田　正**（中央大学理工学部）
共同研究者　研　究　員　**古田　直紀**（中央大学理工学部）
共同研究者　研　究　員　**石塚　盛雄**（中央大学理工学部）
共同研究者　客員研究員　**有馬　敏幸**（本田技術研究所）
共同研究者　客員研究員　**松浦　義則**（広島市立大学情報科学部）
共同研究者　客員研究員　**近藤　矩朗**（東京大学大学院理学研究科）
共同研究者　客員研究員　**劔持　信幸**（千葉大学教育学部）
共同研究者　客員研究員　**高橋　匡康**（宇宙航空研究開発機構）
共同研究者　客員研究員　**岸　恭子**（宇宙航空研究開発機構）

I. Age-dependent spatially distributed two sex model of population dynamics with pair formation and dynamic analysis via computer simulations

ABSTRACT

A two sex model of population dynamics is pretended such that migration and pair formation are extensively taken into account. A characteristic feature of this model is that dynamics of population distributions of single female individuals, male individuals and married pairs is described by a certain nonlocal convective reaction-diffusion system, and that the system is incorporated with nonlinear constraints describing pair formation and dynamic boundary conditions representing birth of new offsprings. A natural class of marriage functions is introduced to better the two sex model. A new method for numerical simulation based on the model is proposed to analyze and predict the dynamics of population. Finally, some computational results are exhibited and compared with statistical data obtained by national surveys in Japan.

KEYWORDS

nonlocal convective reaction-diffusion systems, two sex models of population dynamics, numerical simulation, dynamic boundary condition, pair formation, marriage function.

1 Population dynamics continuous model

Population can be divided into three categories of single males, single females and married couples. We here make an attempt to formulate a mathematical model which describes the movement of population in terms of regional migration and dispersion, birth, marriage, separation, bereavement and mortality. Our habitat may be represented as a domain Ω in the 2D euclidean space $\mathbb{R}^2$. We then write $u \equiv u(t,a,\boldsymbol{x})$ for the population density of single males of age a at time t and location $\boldsymbol{x} \in \Omega$. Likewise, the population density of single females of age b at time t and location $\boldsymbol{x} \in \Omega$ is written as $v \equiv v(t,b,\boldsymbol{x})$. Also, the population density of married couples of age c at time t and location $\boldsymbol{x} \in \Omega$ whose male partners are of age a and female partners are of age b is represented by the function $p \equiv p(t,a,b,c,\boldsymbol{x})$. If time h has passed, then the age of for instance a male becomes $a+h$ and so the rate of change in u is given by

$$\lim_{h\to 0} h^{-1}(u(t+h,a+h,\boldsymbol{x}) - u(t,a,\boldsymbol{x})) = u_t + u_a. \quad (1)$$

In virtue of this, the governing equations of our continuous two sex model are formulated as follows:

$$\begin{aligned} u_t + u_a = {} & \kappa_1 \Delta_x u + \mathbb{E}_1 \cdot \nabla_x u - d_1 u \\ & - \int_0^\infty p(t,a,b,0,\boldsymbol{x})\, db \\ & + \int_0^\infty \int_0^\infty \{\sigma + (1-d_1)d_2\}\, p\, db\, dc, \end{aligned} \quad (2)$$

$$v_t + v_b = \kappa_2 \Delta_x v + \mathbb{E}_2 \cdot \nabla_x v - d_2 v$$

$$- \int_0^\infty p(t,a,b,0,\boldsymbol{x})\,da + \int_0^\infty\int_0^\infty \{\sigma + d_1(1-d_2)\}\,p\,da\,dc, \quad (3)$$

$$p_t + p_a + p_b + p_c = \kappa_3\Delta_x p + \mathbb{E}_3\cdot\nabla_x p - \{d_1(1-d_2) + (1-d_1)d_2 + d_1 d_2 + \sigma\}\,p. \quad (4)$$

Here $d_1 = d_1(t,a,\boldsymbol{x})$ and $d_2 = d_2(t,b,\boldsymbol{x})$ are natural mortality rates of a male and a female, respectively. The coefficient $\sigma = \sigma(t,a,b,c,\boldsymbol{x})$ stands for the separation rate of married couples. The coefficients κ_1, κ_2 and κ_3 represents the regional dispersion rates of single males, single females and married couples, respectively. Moreover, the vector fields $\mathbb{E}_1, \mathbb{E}_2$ and $\mathbb{E}_3$ mean the directions of migration of single males, single females and married couples, respectively. Equations (2) and (3) are the governing equations for the movement of population of single males and females. In each equation, the first term represents dispersion of population in the unit time and the second term stands for migration in the unit time along the vector fields $\mathbb{E}_1, \mathbb{E}_2$ and $\mathbb{E}_3$. The third term represents the mortality rate, the fourth term stands for the marriage function and the fifth term is a loss term due to the separation and bereavement of married couples. Equation (4) is the governing equation for the movement of population of married couples. The first term means the regional dispersion of married couples in the unit time and the second term stands for migration along the vector field $\mathbb{E}_3$ of married couples in the unit time. Finally, the fourth term is a loss term due to the separation and bereavement. Natural constraints in our continuous two sex model are stated below:

$$u(t,0,\boldsymbol{x}) = \int_0^\infty\int_0^\infty\int_0^\infty \beta_1 p\,da\,db\,dc, \quad (5)$$

$$v(t,0,\boldsymbol{x}) = \int_0^\infty\int_0^\infty\int_0^\infty \beta_2 p\,da\,db\,dc, \quad (6)$$

$$p(t,0,b,c,\boldsymbol{x}) = p(t,a,0,c,\boldsymbol{x}) = 0, \quad (7)$$

$$p(t,a,b,0,\boldsymbol{x}) = \psi(u(t,\cdot),v(t,\cdot),p(t,\cdot))(t,a,b,\boldsymbol{x}), \quad (8)$$

$$\frac{\partial}{\partial\boldsymbol{\nu}}u(t,a,\boldsymbol{x})\Big|_{\partial\Omega} = 0, \quad (9)$$

$$\frac{\partial}{\partial\boldsymbol{\nu}}v(t,a,\boldsymbol{x})\Big|_{\partial\Omega} = 0, \quad (10)$$

$$\frac{\partial}{\partial\boldsymbol{\nu}}p(t,a,b,c,\boldsymbol{x})\Big|_{\partial\Omega} = 0. \quad (11)$$

Here $\beta_1 = \beta_1(t,a,b,c,\boldsymbol{x})$ and $\beta_2 = \beta_2(t,a,b,c,\boldsymbol{x})$ are the birth rates of male and female offsprings, respectively. The function ψ is the so-called marriage function that specify the formation of newly married couples. Equations (5) and (6) represent the birth of male and female offsprings, respectively. The boundary values of u at $a = 0$ and v at $b = 0$ on the right-hand sides stand for the population of newborn male and female babies. Boundary condition (7) means that there are no married couples such that the male or female partners are of age 0. Equation (8) is the core of our model and characterize the population of the newly married couples by means of an appropriately chosen marriage function $\psi(u(t,\cdot),v(t,\cdot),p(t,\cdot))(t,a,b,\boldsymbol{x})$. From the mathematical point of view, equations (7) and (8) are interpreted as the boundary conditions for the parameter $p \equiv p(t,a,b,c,\boldsymbol{x})$. Moreover, equations (9) - (11) are the boundary conditions on the boundary of Ω. We here put for simplicity the assumption that there are neither outflow nor inflow of the population through the boundary. This assumption is formulated as a set of the homogeneous Neumann boundary conditions. The initial conditions in our two sex model are formulated as follows:

$$u(0,a,\boldsymbol{x}) = u_0(a,\boldsymbol{x}), \quad (12)$$

$$v(0,b,\boldsymbol{x}) = v_0(b,\boldsymbol{x}), \quad (13)$$

$$p(0,a,b,c,\boldsymbol{x}) = p_0(a,b,c,\boldsymbol{x}), \quad (14)$$

where $u_0(a,\boldsymbol{x})$ means an initial population distribution of single males, $v_0(b,\boldsymbol{x})$ is that of single females and $p_0(a,b,c,\boldsymbol{x})$ stands for an initial population distribution of married couples. The continuous model introduced above improves two sex models which have been proposed so far from various points of view, and it should be mentioned that the proof of the solvability of this continuous model is interesting form the mathematical point of view. In fact, because of the complexity of our model, it is not easy to investigate precise structure and properties of the solutions of this continuous model in an analytical way. On the other hand, it is in general practical to construct approximate numerical solutions and make derail analysis through visualization of the numerical results and comparison with statistical data.

2 Discrete Models

In order to formulate a discrete two sex model of population dynamics, we first introduce a rectangular domain $\Omega \equiv [0, r] \times [0, s]$ as a physical domain. Secondly, the physical domain Ω is discretized by choosing a mesh size $\ell > 0$ and natural numbers M, N such that $2M\ell = r$ and $2N\ell = s$. The mesh size $\ell > 0$ is regarded as a representative distance (or a unit distance) between adjacent grid points. Using the indices

$$m_1 = 0, 1, \cdots, M-2, M-1, \quad m_2 = 0, 1, \cdots, N-2, N-1,$$

we define a computational domain by means of the grid point system

$$\Omega_\ell \equiv \{(m_1\ell, m_2\ell) : m_1 = 0, 1, \cdots, M-2, M-1, \\ m_2 = 0, 1, \cdots, N-2, N-1]\}.$$

We may now formulate a discrete two sex model as a system of finite-difference schemes on the computational domain Ω_ℓ by discretizing the parameters and coefficients involved in the continuous model. The discretization of the time and age variables is obtained by choosing a mesh size $h > 0$ and nonnegative integers i, j, k and n. The mesh size $h > 0$ is regarded as a representative time (a unit time) and also a representative age. In other words, the time t and the ages a, b and c are approximated by ih, jh, kh and nh, respectively. For convenience in notation, we write $A \sim B$ to mean that B is an discrete approximation of A. With this notation the time and age variables are discretized as follows. $a \sim ih, b \sim jh, c \sim kh, t \sim nh$. Once a choice of unit time h is made and the associated discrete approximations are specified, the nth time (year) is simply represented by n, and also the ages of males, those of females and the marital histories are denoted by i, j and k, respectively. The space variable $\boldsymbol{x}$ varying in the domain Ω is discretized by means of the grid points in the computational domain Ω_ℓ in the sense that $\boldsymbol{x} = (x, y) \sim (m_1\ell, m_2\ell) \in \Omega_\ell$.

The principal parameters u, v and p are then discretized as follows:

$$u(t, a, \boldsymbol{x}) \sim u^n_{i,m_1,m_2}, \qquad v(t, b, \boldsymbol{x}) \sim v^n_{j,m_1,m_2},$$
$$p(t, a, b, c, \boldsymbol{x}) \sim p^n_{i,j,k,m_1,m_2}$$

The mortality rates of males and females are discretized as the functions $\mu_{1,i}$ and $\mu_{2,j}$ of the ages of males and females, respectively. Also, the separation rate σ is assumed to be a constant ρ and is discretized in the sense of $\sigma \sim \rho$. In accordance with the governing equations (2)- (4) in the continuous model, the associated discrete governing equations in the computational domain Ω_ℓ for the change in time of the population of single males of age i, that of single females of age j and that of married couples with marital history k are formulated as follows: (2)-(4).

First, the finite-difference operators associated with the diffusion operator Δ and gradient operator ∇ may be defined as follows:

$$\Delta_\ell u^n_{i,m_1,m_2} \equiv \frac{u^n_{i,m_1+1,m_2} - 2u^n_{i,m_1,m_2} + u^n_{i,m_1-1,m_2}}{\ell^2} \\ + \frac{u^n_{i,m_1,m_2+1} - 2u^n_{i,m_1,m_2} + u^n_{i,m_1,m_2-1}}{\ell^2},$$
$$\mathbb{E}_\ell \cdot \nabla_\ell u^n_{i,m_1,m_2} \equiv E_{\ell_x} \frac{u^n_{i,m_1+1,m_2} - u^n_{i,m_1-1,m_2}}{2\ell} \\ + E_{\ell_y} \frac{u^n_{i,m_1,m_2+1} - u^n_{i,m_1,m_2-1}}{2\ell},$$
$$\mathbb{E}_\ell = (E_{\ell_x}, E_{\ell_y}).$$

It should be mentioned here that for the migration operator $\mathbb{E} \cdot \nabla$ up-wind difference schemes should be employed. Although migration processes in the human society is extremely complicated and more appropriate migration operators should be introduced in our model. The operator $\mathbb{E} \cdot \nabla$ may be suitable for describing the migration of microbes. Then the system (2)-(4) are discretized in the form of the following finite-difference system (15)-(17):

$$u^{n+1}_{i+1,m_1,m_2} = \kappa_1 \, \Delta_\ell \, u^n_{i,m_1,m_2} + \mathbb{E}_{\ell 1} \cdot \nabla_\ell u^n_{i,m_1,m_2} \\ + (1 - h\mu_{1,i}) u^n_{i,m_1,m_2} \\ - h^2 \sum_j \Psi(\boldsymbol{w}^n_{i,j,k,m_1,m_2})^n_{i,j,m_1,m_2} \\ + h^3 \sum_{j,k} \{(1 - \mu_{1,i})\mu_{2,j} + \rho\} \, p^n_{i,j,k,m_1,m_2}, \qquad (15)$$

$$v^{n+1}_{j+1,m_1,m_2} = \kappa_2 \, \Delta_\ell \, v^n_{j,m_1,m_2} + \mathbb{E}_{\ell 2} \cdot \nabla_\ell v^n_{j,m_1,m_2} \\ + (1 - h\mu_{2,j}) v^n_{j,m_1,m_2} \\ - h^2 \sum_i \Psi(\boldsymbol{w}^n_{i,j,k,m_1,m_2})^n_{i,j,m_1,m_2} \\ + h^3 \sum_{i,k} \{\mu_{1,i}(1 - \mu_{2,j}) + \rho\} \, p^n_{i,j,k,m_1,m_2}, \qquad (16)$$

$$p^{n+1}_{i+1,j+1,k+1,m_1,m_2} = \kappa_3\ \Delta_\ell\ p^n_{i,j,k,m_1,m_2}$$
$$+\mathbb{E}_{\ell 3}\cdot\nabla_\ell p^n_{i,j,k,m_1,m_2}$$
$$+[1-h\{(1-\mu_{1,i})\mu_{2,j}+\mu_{1,i}(1-\mu_{2,j})$$
$$+\mu_{1,i}\mu_{2,j}+\rho\}]\,p^n_{i,j,k,m_1,m_2}. \quad (17)$$

where $\boldsymbol{w}^n_{i,j,k,m_1,m_2}$ denotes the vector

$$\boldsymbol{w}^n_{i,j,k,m_1,m_2} \equiv (u^n_{i,m_1,m_2}, v^n_{j,m_1,m_2}, p^n_{i,j,k,m_1,m_2}),$$

and $\Psi(\boldsymbol{w}^n_{i,j,k,m_1,m_2})^n_{i,j,m_1,m_2}$ is a discretized marriage function that represents the number of married couples who married in the year of n. Secondly, the finite-difference versions of the boundary conditions (5) - (8) may be given in the following way:

$$u^{n+1}_{0,m_1,m_2} = h^3\sum_{i,j,k}\alpha_{1,j}p^n_{i,j,k,m_1,m_2}, \quad (18)$$

$$v^{n+1}_{0,m_1,m_2} = h^3\sum_{i,j,k}\alpha_{2,j}p^n_{i,j,k,m_1,m_2}, \quad (19)$$

$$p^n_{0,j,k,m_1,m_2} = p^n_{i,0,k,m_1,m_2} = 0, \quad (20)$$

$$p^{n+1}_{i+1,j+1,0,m_1,m_2} = \Psi(\boldsymbol{w}^n_{i,j,k,m_1,m_2})^n_{i,j,m_1,m_2}, \quad (21)$$

Here the birthrates β_1 and β_2 of males and females are both discretized as functions of the ages of female partners of the married couples in the sense that $\beta_1(b) \sim \alpha_{1,j}$ and $\beta_2(b) \sim \alpha_{2,j}$. Also, in this discrete model, the so-called proportionate mixing assumption (see [4]) is employed to formulate the marriage function Ψ, namely,

$$p^{n+1}_{i+1,j+1,0,m_1,m_2} = \Psi(\boldsymbol{w}^n_{i,j,k,m_1,m_2})^n_{i,j,m_1,m_2}$$
$$= \frac{2C_i u^n_{i,m_1,m_2} D_j v^n_{j,m_1,m_2}}{\sum_i C_i u^n_{i,m_1,m_2} + \sum_j D_j v^n_{j,m_1,m_2}}, \quad (22)$$

where C_i and D_j stand for the marriage rates of males of age i and females of age j, respectively.

Finally, the finite-difference versions of the homogeneous Neumann boundary conditions (12)- (13) are formulated on the numerical boundary of the computational domain Ω_ℓ which together describe that there are no incoming and outgoing flows through the numerical boundary.

3 Algorithm of numerical simulation

Numerical simulations based on the discrete model have been performed. We begin by choosing a size of the computational domain. Then the rates of birth, separation, bereavement and mortality are determined in accordance of the statistical data. Also, diffusion and migration coefficients are specified. These rates and coefficients are inserted in the discrete model. We then construct a data set of the initial population distribution u^0_{i,m_1,m_2}, v^0_{j,m_1,m_2} and p^0_{i,j,k,m_1,m_2} by means of statistical data obtained by the census which was performed in a specific year (for instance in 1990 in our case). Starting with the initial values, we apply our discrete model to compute the population of males u^n_{i,m_1,m_2}, that of females v^n_{j,m_1,m_2} and that of married couples p^n_{i,j,k,m_1,m_2} in the year of n. The algorithm may be described as follows:

First, constituent constants and rates mentioned above are specified in the model and the computational domain Ω_ℓ is initialized by assigning the initial population data on all of the grid points in the computational domain. Second, an iteration number N of computation is specified and numerical computation is made N times through the finite- difference scheme (15)-(17) and the finite-difference boundary conditions (18)- (22) with respect to the age variables a, b and c. Third, the computational results are saved on the computational domain in each step of iteration since the numerical results are visualized to investigate the movement of population. The finite-difference versions of the homogeneous Neumann boundary conditions (12)-(13) are necessary to make numerical computations iteratively on the computational domain Ω_ℓ and these discrete boundary conditions guarantee that both of the inflow and outflow remain to be 0.

4 Results of numerical simulation

Applying the discrete two sex model presented above and using statistical data obtained through the 1990 national survey in Japan, we have performed numerical simulations to predict the movement of population every five years up to 2010.

The movement of population in Japan is investigated every five years, and it was confirmed that our numerical results for the year of 2000 agree with the statistical data. The following figures depict our numerical results and show the age structure of population in terms of

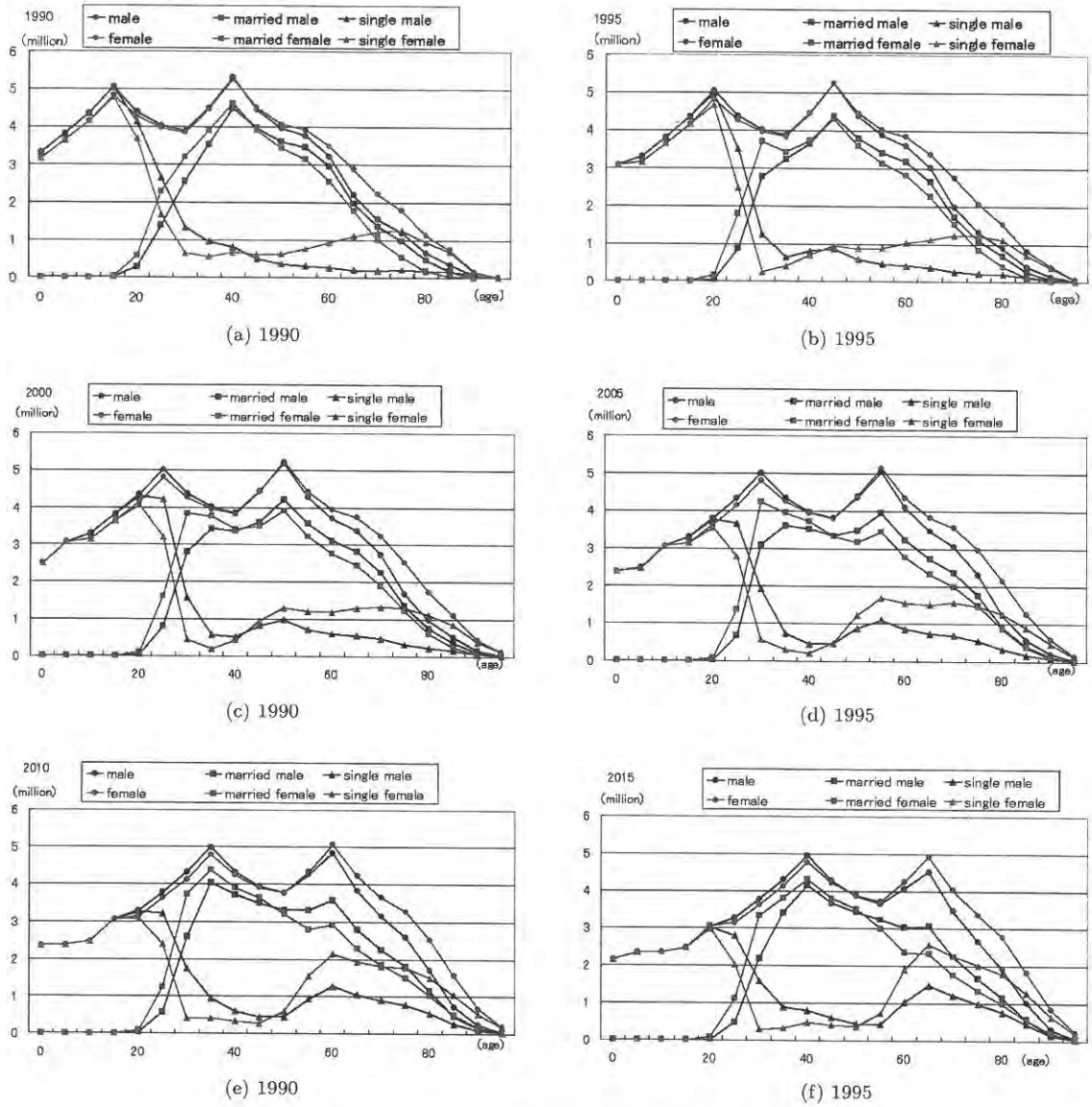

Fig 1 Populations of single males, single females and married couples

single female and male individuals, married female and male individuals, and movement of total population. In Figure 1 initial populations are given in (a) and the results of computer simulations at an interval of years.

References

[1] K. P. Hadeler, "Pair formation in age-structured populations," *Acta. Applic. Math.*, No.14, pp.91–102, 1989.

[2] T. Matsumoto, S. Oharu and H. R. Thieme, "Nonlinear perturbations of a class of integrated semigroups," *Hiroshima Math. J.*, No.26, pp.433–473, 1996.

[3] T. Matsumoto, S. Oharu and K. Shitaoka, "On the semigroup approach to age-dependent spatially distributed two sex models of population dynamics," *Adv. Math Sci. Appl.*, **13**, No.2 (2003), 423–442.

[4] A. Inaba, *Mathematical Demography* (in Japanese), Tokyo University Press, 2002.

[5] Toshitaka Matsumoto, Shinnosuke Oharu and Koichi Shitaoka, "On the semigroup approach to age-dependent apatially distributed two sex models of population dynamics" Advance in Mathematical Science and Applications, Vol.13, No.2 pp423–442, (2003).

環境流体における移流拡散反応現象の数理モデリングと環境科学への応用

研究代表者　研　究　員　**大春慎之助**（中央大学理工学部）
共同研究者　研　究　員　**杉山　高一**（中央大学理工学部）
共同研究者　研　究　員　**松下　貢**（中央大学理工学部）
共同研究者　研　究　員　**山田　正**（中央大学理工学部）
共同研究者　研　究　員　**古田　直紀**（中央大学理工学部）
共同研究者　研　究　員　**石塚　盛雄**（中央大学理工学部）
共同研究者　客員研究員　**有馬　敏幸**（本田技術研究所）
共同研究者　客員研究員　**松浦　義則**（広島市立大学情報科学部）
共同研究者　客員研究員　**近藤　矩朗**（東京大学大学院理学研究科）
共同研究者　客員研究員　**劔持　信幸**（千葉大学教育学部）
共同研究者　客員研究員　**高橋　匡康**（宇宙航空研究開発機構）
共同研究者　客員研究員　**岸　恭子**（宇宙航空研究開発機構）

II. An ecological model for red tide plankton and numerical simulation

ABSTRACT

In recent years, mass mortality of bivalves such as oysters has been caused by red tide plankton named Heterocapsa Circularisquama. Heterocapsa are vegetative plankton and cause serious damage to fishery in the coastal ocean. Therefore, it is urgent to elucidate the ecosystem of Heterocapsa in order to predict the formation of red tides. In this paper a new ecological model is presented to describe the complex ecosystem of Heterocapsa and show that phase variation of diatom species and generation processes of nutrients are important factors to be taken in the ecological model. The validity of the model is examined by comparing the numerical results with observational data.

KEYWORDS

mathematical ecological model, ecosystem of red tide plankton, geophysical model for coastal ocean, numerical simulation, three dimensional visualization.

1 Ecological factors of microbes in the ocean

Red tides of Heterocapsa Circularisquama take place in the period from August through October. Heterocapsa are vegetative plankton and form red tides at comparatively high temperatures and high salinity of sea water. The living state of this species is affected by physical conditions of the coastal ocean. The red tides cause mass mortality of bivalves in such a way that their clapping motion is weakened and the bivalves die after opening their shells. Therefore it is urgent to make detailed ecological studies of this species and elucidate the outbreak of red tides.

The coastal ocean is considered complex multicomponent fluid and the ecology of Heterocapsa is affected by other living things and supported by physical state of the coastal ocean which depends on seasonal variations, air-sea interaction, weather, water temperature, salinity and water currents. Since the water currents consist mostly of turbulent flows, it is not straightforward to investigate the ecosystem of Heterocapsa in the ocean. In this paper the most advanced pieces of information obtained in the related fields are combined from the point of view of mathematical modeling and a mathematical model describing these biological phenomena is presented in conjunction with an appropriate geophysical model which specifies the structure and dynamics of the coastal ocean. It is also emphasized that computer simulations using such models are particularly effective for investigating such nonlinear phenomena in a systematic and comprehensive way.

The mathematical model is formulated by combining a biological model involving various environmental factors as constituent parameters with a geophysical model which describes the dynamics of the coastal ocean. Our

model for the ecosystem incorporates evolution equations for the cell populations of vegetative and animal plankton u, v, and w, concentration of nutrients and dissolved oxygen N, N^*, α, β, density distributions of detritus and sediment γ, and σ. The rates of change over time of these parameters are governed by diffusion processes, transport processes along water currents, biological and biochemical reactions.

2 Ecological models

Our mathematical model consists of nonlinear convective reaction- diffusion equations and boundary conditions. The convective reaction diffusion system represent the change in time of the density of Heterocapsa u , active diatom species v, resting diatom species v^*, animal plankton w, oxidized nutrients (oxidized nitrogen) N, ammonium material N^*, detritus α, dissolved oxygen β, dissolved carbon dioxide γ and the sum of sediments S, respectively. Heterocapsa use their flagella for the so-called diurnal vertical motion and are transported by water currents and the diffusion effects in the ocean.

2.1 Heterocapsa Circularisquama

The proliferation is affected by photosynthesis, the ingestion of oxidized nutrients and competition with with activated diatoms species. Heterocapsa are vegetative plankton, and they are predated by animal plankton. Also, they die because of natural mortality. The change in time of the cell density of Heterocapsa $u \equiv u(t,x,z)$ at location (x,z) and time t is governed by the following equation:

$$\begin{aligned} u_t = &(C_u u_x)_x + (D_u u_z)_z - (Vu)_x - (Wu)_z - (Ku)_x \\ &- (Lu)_z - \left(\hat{K}u\right)_x - \left(\hat{L}u\right)_z \\ &+ R_u N^* u(a_1 - a_2 u - a_3 v) - \bar{R}_w w u - M_u u \end{aligned} \quad (1)$$

Here $C_u, D_u, V, and W$ represent diffusion coefficients and convective flow components in the x and z directions. Also, $K, L, \hat{K}, and \hat{L}$ denote the rates of motion due to photosynthesis and precipitation at night in the x and z directions, respectively. The coefficients a_1, a_2, a_3 stand for the rates of natural proliferation, self-competition, and competition with diatom species. The coefficients $\bar{R}_w$ and M_u stand for the rate of predation of animal plankton and that of mortality of Heterocapsa.

2.2 Diatom species in the activated phase

Activated diatom species are transported by water currents and the natural diffusion in the ocean. Their proliferation is affected by photosynthesis, the ingestion of oxidized nutrients and competition with Heterocapsa. The loss of their population is due to the predation by animal plankton and natural mortality in the same way as in Heterocapsa. Activated diatom species transmute from activated phase into resting phase and conversely from resting phase into activated phase in accordance with environmental conditions such as the density of oxidized nutrients, that of dissolved oxygen and light intensity. The change in time of the cell density of activated diatom species at location (x,z) and time t may be characterized by the following equation:

$$\begin{aligned} v_t = &(C_v v_x)_x + (D_v v_z)_z - (Vv)_x - (Wv)_z \\ &+ R_v N v(b_1 - b_2 v - b_3 u) - R_w w v \\ &- M_v v + \phi(N, L, \beta) v^* - \psi(N, L, \beta) v \end{aligned} \quad (2)$$

Here C_v and D_v are diffusion coefficients in the x and z directions, and the constants b_1, b_2, and b_3 represent the rates of proliferation, self-competition and competition with Heterocapsa of the activated diatom species. The coefficients R_w and M_v are the rates of predation by animal plankton and that of mortality of activated diatom species. Moreover, the functions ϕ, ψ represent the rates of phase succession from the activated phase into the resting phase and that from the resting phase into the activated phase, respectively.

2.3 Diatom species in the resting phase

Diatom species in the resting phase are transported by water currents and the diffusion effects in the ocean. The resting diatom species do not ingest nutrients and do not proliferate. The population decrease is due to the predation by animal plankton and the natural mortality. Moreover, the phase variation from the activated phase into resting phase and that from the resting phase to activated phase are motivated by the environmental factors such as oxidized nutrients, dissolved oxygen and light intensity. In view of the above-mentioned observation, the change in time of the cell density of the resting diatom species at location (x,z) and time t is described

by the following equation:

$$v_t^* = (C_v^* v_x^*)_x + (D_v^* v_z^*)_z - (Vv^*)_x - (Wv^*)_z - R_w^* w v^* - M_v^* v^* - \phi(N, L, \beta) v^* + \psi(N, L, \beta) v - \phi^*(N, L, \beta) v^* \quad (3)$$

Here the coefficients C_{v^*} and D_{v^*} are diffusion coefficients in the x and z directions. The constant R_w^* represents the rate of predation by animal plankton and M_v^* denotes the mortality rate of resting diatom species. The function ϕ^* is the rate of phase variation from resting phase to the activated phase.

2.4 Proliferation rates of Heterocapsa and diatom species

Vegetative plankton proliferates at night of the day on which they get sufficient amount of daylight. In accordance with these facts, the proliferation rates of Heterocapsa u and activated diatom species v are essentially affected by the effect of photosynthesis during the daytime and the amount of consumed oxygen. Here we assume that the proliferation rates R_u and R_v of Heterocapsa and activated diatom species are specified by the following equations, respectively.

$$R_u = R_u(L, \beta) = \frac{2c_U d_U L\beta}{c_U L + d_U \beta},$$
$$R_v = R_v(L, \beta) = \frac{2c_V d_V L\beta}{c_V L + d_U \beta} \quad (4)$$

2.5 Animal plankton

Animal plankton do not have capability of motion, and they are transported only by water currents and diffusion effects in the ocean. They proliferate by predating on vegetative plankton such as Heterocapsa and diatom species. For these life activities they consume dissolved oxygen, although they are assumed to die with a natural mortality in a way similar to other kinds of plankton. In view of the above-mentioned, the change in time of the cell density of animal plankton $w \equiv w(t, x, z)$ at location (x, z) and time t is described by the following equations:

$$w_t = (C_w w_x)_x + (D_w w_z)_z - (Vw)_x - (Ww)_z + \bar{R}_w w u + R_w w v + R_w^* w v^* + P_w(\beta) w - M_w w \quad (5)$$

Here C_w, D_w are the diffusion coefficients in the x and z directions, P_w stands for the proliferation rate of animal plankton which may depend upon the distribution of dissolved oxygen and M_w means the mortality rate of animal plankton.

2.6 Deoxidized nitrogens

Reduced nutrients such as deoxidized nitrogens were mainly ingested by Heterocapsa and are transported by water currents and the diffusion processes in the ocean. These kinds of nutrients are produced through the decomposition of detritus and sediments on the sea bed in the oxygen-deficient water mass. Such nutrients are also supplied from the river and are sometimes changed to oxidized nitrogens by specific bacteria such as nitrosomonss sp. In view of the above-mentioned, the change in time of the density of reduced nutrients $N^* \equiv N^*(t, x, z)$ at location (x, z) and time t is characterized by the following equation:

$$N_t^* = (C_N^* N_x^*)_x + (D_N^* N_z^*)_z - (VN^*)_x - (WN^*)_z + R_\alpha^*(\beta)\alpha + R_S^*(\beta) S - R_u N^* u(a_1 - a_2 u - a_3 v) - \eta(L, \beta) N^* + S_R^*. \quad (6)$$

Here C_N^* and D_N^* are the diffusion coefficients in the x and y directions. The coefficients $R_\alpha^*.R_S^*$ are the rates of decomposition of detritus and sediment, The coefficient η stands for the rate of chemical change of reduced nutrients to the oxidized nitrogens and S_R^* means the supply of ammonium ions from the river.

2.7 Oxidized nitrogens

Diatom species mainly ingest oxidized nutrients which are transported by water currents and the diffusion effects in the ocean. In context with reduced nutrients, oxidized nutrients such as oxidized nitrogens are supplied from not only the river but also they are produced under the circumstances that oxygen is sufficiently supplied. In accordance with physical and chemical conditions in the ocean, oxidized nutrients can be changed to inorganic compounds such as nitrogen gas. In view of these factors, the change in time of the density of oxidized nutrients $N \equiv N(t, x, z)$ at location (x, z) and time t is described by the following equation:

$$N_t = (C_N N_x)_x + (D_N N_z)_z - (VN)_x - (WN)_z + R_\alpha(\beta)\alpha + R_S(\beta) S - R_v N v(b_1 - b_2 v - b_3 u) + \phi^*(N, L, \beta) v^* + \eta(L, \beta) N^* + S_R. \quad (7)$$

Here C_N, D_N are the diffusion coefficients in the x and z directions. The coefficients R_α, R_S are the rate of decomposition of detritus and sediment, and S_R means the sum of supplies of the oxidized nutrients from the river.

2.8 Detritus

Detritus are dead bodies of plankton and are transported by water currents and the diffusion processes in the ocean. They are dissolved into oxidized nutrients or dioxidized nitrogens by bacteria in the ocean. In view of these facts, the change in time of the density of detritus at location (x, z) and time t is described by the following equation:

$$\begin{aligned}\alpha_t = &(C_\alpha \alpha_x)_x + (D_\alpha \alpha_z)_z - (V\alpha)_x - (W\alpha)_z \\ &-R_\alpha^* (\beta)\, \alpha - R_\alpha (\beta)\, \alpha \\ &+M_u u + M_v v + M_v^* v^* + M_w w. \end{aligned} \tag{8}$$

Here C_α, D_α are the diffusion coefficients in the x and z directions.

2.9 Dissolved oxygen

Oxygen is transported by water currents and the diffusion effects in the ocean. Oxygen is generated through the photosynthesis by vegetative plankton and is supplied from the free surface of the ocean depending upon temperature, wind, atmospheric pressure and rain. On the other hand, oxygen is consumed and carbon dioxide is generated when detritus and sediment on the sea bed are dissolved. In this way, oxygen plays an important role in life activities as well as the related biological and biochemical phenomena. In view of these factors, the change in time of the density of dissolved oxygen $\beta \equiv \beta(t, x, z)$ at location (x, z) and time t is characterized by the following equations:

$$\begin{aligned}\beta_t = &(C_\beta \beta_x)_x + (D_\beta \beta_z)_z - (V\beta)_x - (W\beta)_z \\ &+ \left(Pu + \bar{P}v\right)\gamma - \left(R_\alpha (\beta)\, \alpha + R_S (\beta)\, S\right) \\ &- \left(R_\alpha^* (\beta)\, \alpha + R_S^* (\beta)\, S\right) + S_A. \end{aligned} \tag{9}$$

Here C_β, D_β are the diffusion coefficients in the x and z directions. The coefficients $P, \bar{P}$ represent the rate of supply of oxygen by photosynthesis by Heterocapsa and diatom species, respectively. The term S_A represents the sum of supplies of oxygen from the free surface of the ocean.

2.10 Carbon Dioxide

Carbon dioxide is transported by water currents and the diffusion processes in the ocean in the same way as in oxygen and is dissolved in the ocean depending upon temperature, atmospheric pressure, winds, and rainfall. In contrast with oxygen, carbon dioxide is consumed through photosynthesis by vegetative plankton. Taking these things into consideration, the change in time of the density of dissolved carbon dioxide $\gamma \equiv \gamma(t, x, z,)$ at location (x, z) and time t is characterized by the following equation:

$$\begin{aligned}\gamma_t = &(C_\gamma \gamma_x)_x + (D_\gamma \gamma_z)_z - (V\gamma)_x - (W\gamma)_z \\ &- \left(Pu + \bar{P}v\right)\gamma + S_A^* \end{aligned} \tag{10}$$

Here C_γ, D_γ are the diffusion coefficients in the x and z directions. The coefficients $P, \bar{P}$ are the rates of consumption of carbon dioxide through photosynthesis by Heterocapsa and diatom species. The term S_A^* represents the sum of supplies of carbon dioxide from the free surface of the ocean.

2.11 Sediment on the sea bottom

Detritus precipitates into the sediment on the sea bed and are dissolved by various types of bacteria. In view of this, the change in time of the density of sediment $S \equiv S(t, x, z)$ at location (x, z) and time t is specified by the following equation:

$$S_t = \alpha_z - R_s S \tag{11}$$

The change in time of the densities of oxidized and reduced nutrients generated on the sea bed are represented by the two equations below:

$$\begin{aligned} N_t^* &= R_\alpha^* (\beta)\, \alpha + R^* (\beta, \gamma)\, S, \\ N_t &= R_\alpha (\beta)\, \alpha + R (\beta, \gamma)\, S \end{aligned} \tag{12}$$

3 Numerical discrete model

In a continuous model, the parameters are assumed to be functions of position (x, y, z) in a 3D domain Ω and time t. Here space and time are discretized as (il, jl, kl) and nh, where $l, h > 0$ are appropriately chosen space and time increments, respectively. In accordance with this discretization, the parameters are also discretized in the (vector) form as:

$$\mathbf{U}^n \equiv \mathbf{U}_{i,j,k}^n$$

$$\equiv [u^n, v^n, v^{*n}, N^n, N^{*n}, w^n, \alpha^n, \beta^n, \gamma^n, \sigma^n]_{i,j,k} \quad (13)$$

and the discrete governing equation is formulated in the form

$$h^{-1}[\mathbf{U}^n - \mathbf{U}^{n-1}] = D\Delta_l \mathbf{U}^n + \mathbf{V}_\mathbf{l} \cdot \nabla_l \mathbf{U}^n + \mathbf{R}_\mathbf{l}(n, i, j, k, \mathbf{U}^{n-1}), \quad (14)$$

where $D\Delta_l$ denotes a difference diffusion operator, $\mathbf{V}_\mathbf{l} \cdot \nabla_l$ represents a difference convection operator and $\mathbf{R}_\mathbf{l}$ stands for a vector form of the reaction terms. For instance the first and fourth components of $\mathbf{R}_\mathbf{l}$ associated with the rates of change over time of u and N take the forms

$$R_u N^* u^n (a_1 - a_2 u^n - a_3 v^n) - \bar{R}_w w^n u^n - M_u u^n, \quad (15)$$

$$R_\alpha(\beta)\alpha + R_S(\beta) S - R_v N v^n (b_1 - b_2 v^n - b_3 u^n) + \phi^*(N, L, \beta) v^* + \eta(L, \beta) N^* + S_R \quad (16)$$

Therefore the rate of change over time of the cell population of Heterocapsa is determined by the diffusion processes in the ocean, advection along water currents, light intensity in the daytime and precipitation at night, and biological interactions based on the proliferation which is affected by photosynthesis and nutrients, competition with diatom species, predation by animal plankton, and mortality. The reaction terms (16) for oxidized nutrients specify the generation processes.

4 Numerical simulations

In order to perform numerical simulations based on the continuous model introduced in Section 2, an approximate discrete scheme has been formulated by means of finite-difference schemes and numerical computations have been made in the following way: We first fix a 2D computational rectangular domain in such a way that the upper horizontal side corresponds to the free surface of the ocean and the lower horizontal side is associated with the sea bottom, and such that the horizontal and vertical sides are parallel to the x and z axes, respectively. For the formulation of a numerical model which describes this complex biological phenomena, we necessitate specifying adequate numerical values of the coefficients and choosing ecologically right initial data that are usually determined in accordance with observational data at the initial time as well as indirectly predicted environmental parameters. By virtue of the numerical data at a time step n of the iterative computations, numerical results for the $n+1$th step are obtained through the discrete scheme to describe the distributions of cell densities of plankton and concentration of nutrients. Our model does not explicitly contain terms and coefficients which describe weather conditions and physical states of the ocean. Although these conditions are implicit in the model, such coefficients and state parameters can be specified to reflect the weather conditions and physical marine states. Therefore suitable numerical values should be chosen for the coefficients in such a way that the coefficients are accurately affected by those physical states of the region under consideration. In the same way, seasonal variations are also taken into the model by changing the coefficients in an appropriate way.

In order to choose optimal values for the coefficients, we necessitate specifying characteristic values by investigating the dependence of the model on the choice of optimal combinations of parameters and coefficients. Such dependence is strongly affected by the regional characteristics. In our numerical simulations we chose Etajima Bay in Hiroshima, Japan, which is a small sized closed bay connected through a narrow channel with the outside ocean and employed observational data taken in the year of 1999. After detailed investigation into the dependence of the model on the coefficients, we performed numerical simulations to reproduce the red tide formation in the bay which took place in 1999 and was witnessed by the fishermen. In accordance with the results and information obtained by our simulations, characteristic values of the coefficients have been specified and careful studies in the dependence of the model on the coefficients have been made.

5 Numerical simulations and their visualization

In our new model (1)-(2) phase variation of diatom species and generation processes of nutrients are expensively taken into account. We then perform numerical simulations based on this model to reproduce typical red tide formation which took place in 1999 in Setouch

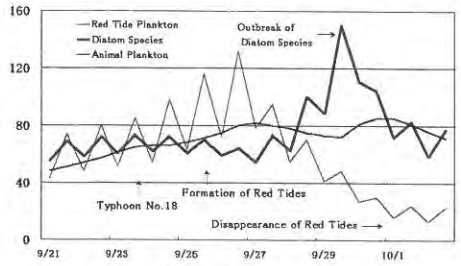

Fig.1 Observational results in Etajima Bay

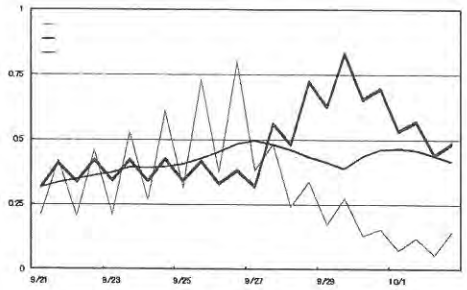

Fig.2 Results of numerical simulations

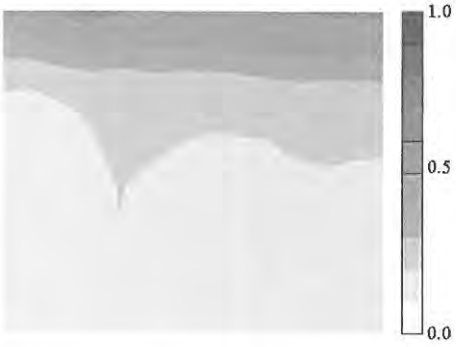

Fig.3 Distribution of Heterocapsa in the daytime

Fig.4 Distribution of Heterocapsa at night

Inland Sea, Japan.

Figures 1 and 2 depict the numerical results which together show the diurnal vertical motion of Heterocapsa. The present model improves our previous model proposed in 2001 in the sense that the relationships between the coefficients involved in the model have been clarified and dependence of the constituent parameters on those coefficients can be studied more accurately. Also, time evolution of the microbes under consideration and generation processes of nutrients are formulated in the model in a more precise way so that results of numerical simulations can be obtained in a natural way.

References

[1] S. Oharu, Y. Taniguchi and M. Yamaguchi, "Ecological Models of Red Tide Plankton and Computer Simulation," Proc. of the Eurosim 2001 conference, Shaping Future with Simulation 2001.

環境流体における移流拡散反応現象の数理モデリングと環境科学への応用

研究代表者　研　究　員　**大春慎之助**（中央大学理工学部）
共同研究者　研　究　員　**杉山　高一**（中央大学理工学部）
共同研究者　研　究　員　**松下　　貢**（中央大学理工学部）
共同研究者　研　究　員　**山田　　正**（中央大学理工学部）
共同研究者　研　究　員　**古田　直紀**（中央大学理工学部）
共同研究者　研　究　員　**石塚　盛雄**（中央大学理工学部）
共同研究者　客員研究員　**有馬　敏幸**（本田技術研究所）
共同研究者　客員研究員　**松浦　義則**（広島市立大学情報科学部）
共同研究者　客員研究員　**近藤　矩朗**（東京大学大学院理学研究科）
共同研究者　客員研究員　**劔持　信幸**（千葉大学教育学部）
共同研究者　客員研究員　**高橋　匡康**（宇宙航空研究開発機構）
共同研究者　客員研究員　**岸　　恭子**（宇宙航空研究開発機構）

III. Flow analysis around structures in environmental fluids and its application to environmental restoration technology

ABSTRACT

Importance and application of numerical flow analysis in environmental science and technology are outlined. Fluid phenomena in the ocean, rivers, atmosphere and the ground are investigated by means of numerical methods and in turn proposals for the control, restoration and counterplans against the so-called environmental disrupters which destroy natural environment as well as ecological systems in nature. All such environmental disrupters diffuse in and are transported by environmental fluids. Those disrupters sometimes react on some other chemicals to generate more poisonous materials. Environmental fluid dynamics is effective for the evaluation, prediction and restoration of the environmental damage. In this paper a mathematical model of environmental fluid is presented and results of numerical simulations based on the model are exhibited.

KEYWORDS

Environmental fluid, computational fluid dynamics, numerical simulation, environmental restoration technology, three dimensional visualization.

1 Environmental fluids and environmental restoration technology

Fluid dynamical technologies are increasingly becoming important in the field of environmental science and technology. Evaluation of environmental fluid flow using numerical methods is particularly useful to understand the complex fluid motion and make it possible to control the flow fields from the point of view of environmental restoration. The environmental fluid problems may be classified by three types of applications. The first application is concerned with ultimate use of exergy. This is the most important subject for existing engine that use fossil fuel for combustion. Secondly, new energy sources such as wind and wave power generation should be extensively researched and developed. Thirdly, it is indispensable to develop not only efficient and harmless energy sources but also technologies to restore the environment which has already been polluted by exhaust gases through combustion of fossil fuel. It is also important to develop effective methods for protecting the environment fluids against pollutants. In this paper the field of studies in evaluation, control and prediction of transport phenomena which arise in a variety of environmental problems is called *environmental fluid dynamics*. Obviously, the environmental fluid dynamics is one of the key theories to invent efficient technologies for the preservation and restoration of the natural environment. Here we focus our attention on a dynamical analysis of diffusion and transport processes

of pollutants in environmental fluids. A mathematical model of environmental fluids is presented and results of simulations are exhibited. It is then expected that new environmental restoration technology will be developed.

2 A mathematical model of environmental fluids

As a mathematical model describing the motion of environmental fluids, we employ the compressible Navier-Stokes system. Although it is known (see [1]) that the application of numerical methods for the compressible Navier-Stokes system to low-speed flows does not necessarily provide us with satisfactory results on the convergence. This fact implies that numerical simulations become inefficient and the associated computational results turn out to be inaccurate. These numerical difficulties are caused by the circumstances that the characteristic velocities in the compressible Navier-Stokes systems are convective and sound speeds, and so that their ratios become large and the so-called stiffness of the system may occur due to the disparity of eigenvalues of the system. One of efficient counter measures for those numerical difficulties is to employ the so-called Boussinesq approximation under the assumption that the ratio of the change in density to that of temperature. In fact, under the Boussinesq approximation numerical methods which have been developed for incompressible fluids can directly applied. On the other hand, in the case that the ratio of the change in density to that of temperature is considerably large, the low Mach number approximation is proposed in [4].

In this paper we apply the Boussinesq approximation to the Navier-Stokes system and formulate the following system of equations (1-3) as our mathematical model for describing the motion of environmental fluids:

$$\nabla \cdot \mathbf{v} = 0 \tag{1}$$

$$\rho\left[\mathbf{v}_t + (\mathbf{v}\cdot\nabla)\mathbf{v}\right] = -\nabla p + \mu\Delta\mathbf{v} - \rho\beta(T - T_0)\mathbf{g} \tag{2}$$

$$\rho Cp\left[T_t + (\mathbf{v}\cdot\nabla)T\right] = \nabla(\kappa\nabla T) + S_c \tag{3}$$

Here the parameters $\mathbf{v}$, ρ, p, μ, β, $\mathbf{g}$, T and T_0 represent the velocity vector, density, pressure, viscosity coefficient, rate of volume expansion, the acceleration of gravity, temperature and its reference temperature, respectively. Also, the coefficient κ means the thermal conductivity and S_c stands for the sum of heat sources in the fluid.

Our main objective here is to get numerical data describing the flow field around bodies in an environmental fluid under consideration. For this purpose we impose Dirichlet boundary conditions for $\mathbf{v}$ and T and homogeneous Neumann boundary conditions for p on the inflow boundary. On the outflow boundary we impose homogeneous Neumann conditions for $\mathbf{v}$, T and Dirichlet boundary conditions for p. On the surface of each body standing in the fluid, we impose the non-slip conditions for $\mathbf{v}$ and homogeneous Neumann conditions for T and employ an inhomogeneous Neumann boundary conditions for p which is obtained from equation (2). In this paper a new numerical scheme is proposed such that an fully implicit Euler scheme for the numerical velocity is involved.

3 Numerical Model

Making discretization in time of (1) by use of the Euler implicit method, we obtain the following system of equations:

$$\nabla \cdot \mathbf{v}^{n+1} = 0 \tag{4}$$

$$\frac{\mathbf{v}^{n+1} - \mathbf{v}^n}{\Delta t} = -(\mathbf{v}^{n+1}\cdot\nabla)\mathbf{v}^{n+1} - \frac{1}{\rho}\nabla p^{n+1} + \frac{\mu}{\rho}\Delta\mathbf{v}^{n+1} - \beta(T^{n+1} - T_0)\mathbf{g} \tag{5}$$

$$\frac{T^{n+1} - T^n}{\Delta t} = -(\mathbf{v}^{n+1}\cdot\nabla)T^{n+1} + \frac{1}{\rho C_p}\nabla(\kappa\nabla T^{n+1}) + Sc \tag{6}$$

In what follows, we regard equations (4)-(6) as the governing equations for the motion of numerical fluids and then take the standpoint that the numerical solvability of this basic model is to be investigated. In view of the unilateral positive direction of time, we linearize the nonlinear term on the right-hand side of (5) as $(\mathbf{v}^{n+1}\cdot\nabla)\mathbf{v}^{n+1} \simeq (\mathbf{v}^{n}\cdot\nabla)\mathbf{v}^{n+1}$ we obtain the following Helmholtz equation for the velocity vector $\mathbf{v}^{n+1}$:

$$\left[1 + \Delta t(\mathbf{v}^{\mathbf{n}}\cdot\nabla)\right]\mathbf{v}^{n+1} - \frac{\mu\Delta t}{\rho}\Delta\mathbf{v}^{n+1} = \mathbf{v}^n - \frac{\Delta t}{\rho}\nabla p^{n+1} - \beta\Delta t(T^{n+1} - T_0)\mathbf{g} \tag{7}$$

Substituting equation (5) into equation (4), Poisson's equation for the pressure field p^{n+1} is obtained:

$$\Delta p^{n+1} = -\rho\left[\nabla\cdot\left\{(\mathbf{v}^{n+1}\cdot\nabla)\mathbf{v}^{n+1}\right\} - \frac{\nabla\cdot\mathbf{v}^n}{\Delta t}\right] - \rho\beta(T^{n+1} - T_0)\nabla\cdot\mathbf{g} \tag{8}$$

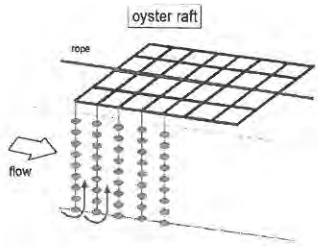

(a) Oyster raft

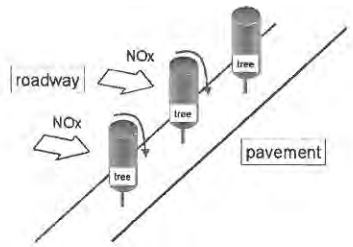

(b) Street trees

Fig 1 Structures in the ocean and atmosphere

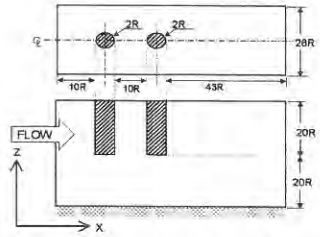

(a) Settings of computational domain

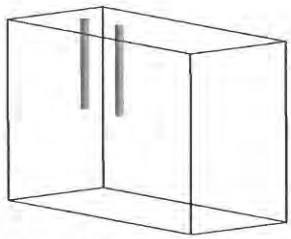

(b) 3D view of computational domain

Fig 2 Settings for numerical simulation

Also, the Helmholtz equation for the temperature field is obtained from equation (6) in the following form:

$$[1+\Delta t(\mathbf{v}^{\mathbf{n}}\cdot\nabla)]\,T^{n+1}-\frac{\kappa\Delta t}{C_p\rho}\boldsymbol{\Delta}T^{n+1}=T^n+\Delta tSc \quad (9)$$

Elliptic equations (7), (8) and (9) are discretized with respect to the space variables and the resultant system of finite-difference equations are solved by applying an appropriate iteration method. Namely, given velocity field $\mathbf{v}^n$, pressure field p^n and temperature field T^n at the nth time step, the velocity field $\mathbf{v}^{n+1}$, pressure field p^{n+1} and temperature field T^{n+1} are obtained at the $(n+1)$th step through the iteration procedures, respectively. As to the discretization of the physical space Ω, we employ a collocation form such that the scalar and vector quantities on the same grid points. For the discretization of the convective terms, we apply an up-wind scheme of the third order accuracy which is proposed in Kawamura [2]:

$$v\left(\frac{\partial v}{\partial x}\right)_i = v_i\frac{-v_{i+2}+8(v_{i+1}-v_{i-1})+v_{i-2}}{12h} + |v_i|\frac{v_{i+2}-4v_{i+1}+6v_i-4u_{i-1}+v_{i-2}}{4h} \quad (10)$$

For other terms we employ central difference schemes of the second order accuracy. It should be mentioned here that the above-mentioned finite- difference scheme is unconditional stable.

4 Settings of Numerical Simulation

We here discuss flow analysis around cylinders with bottom ends standing in an environmental fluid. In the numerical simulations we have performed, flow analysis was made for a typical fluid flow. Our setting may be outlined as follows: We consider a parallelepiped region $\mathbf{R}$ in $\mathbb{R}^3$ and assume that one side is the inflow boundary and the opposite side is the outflow boundary. We then insert two circular cylinders with radius 1R and length 20R both of which have bottom ends in the region $\mathbf{R}$ in such a way that they are arranged in a row at an interval of 10R and perpendicular to the top side of $\mathbf{R}$, as illustrated in Figure 2. For convenience, we call the cylinder facing the inflow boundary the front cylinder and the cylinder facing the outflow boundary the rear cylinder. In this setting we performed numerical simulations and made detailed analysis around the two cylinders parallel to each other. One of the typical applications of this analysis is the simulation of the behavior of red tide plankton in a neighborhood of the farming part of an oyster raft floating on the ocean, as illustrated in Figure 1(a). Another application is the study in the effect and influence of convective diffusion phenomena of automobile exhaust fumes on roadside trees, as shown in Figure 1(b). Numerical conditions are put in the following way: The Reynolds number

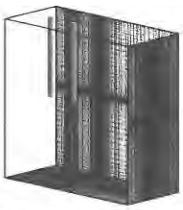

(a) 3D general view

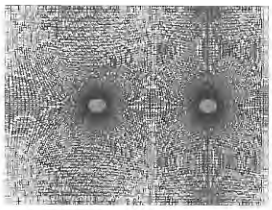

(b) Grid points around the circular cylinders

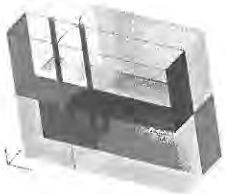

(c) Grid decomposition for parallel computation

Fig 3 Grid point system

$(= \rho|\mathbf{v}|2R/\mu)$ in accordance with the main flow velocity is assumed to be $Re = 2500$ and the temperature distribution is assumed to follow a linear distribution such that $T = 300K$ on the top of the front cylinder and $T = 290K$ under the bottom end.

5 Generation of Grid Point Systems

In order to obtain numerical solutions, we first define grid point system fitting with the surfaces of the bodies and compute solutions of discretized equations consistent with (1)- (3) on the grid points. Here an effective method for generating grid point systems which fit the surfaces of bodies in the fluid is proposed, and it is demonstrated that a simulation code can be developed on the grid point system. We generate grid point systems not only on the region of the fluid but also in the inside of the bodies so that those grid point systems are connected continuously on the boundaries of the bodies. Therefore the final grid point system covers a simply connected domain on which simulations are performed. A concrete procedure for generating such grid point system may be outlined as follows: Firstly, on each horizontal plane crossing the cylinders, we divide the computational domain into the inside and outside of the circles which are cross sections of the cylinders and then subdivide the outside of the circles into a finite number of simply connected subdomains. Secondly, we generate initial grid point systems on each subdomain by algebraic methods and then construct a spatial smooth grid point system by solving the associated elliptic system in a numerical sense.

Let $\xi = \xi(x, y)$ and $\eta = \eta(x, y)$ denote the mapping from the physical domain into the computational domain. Basics of this method is that, following Thompson et al. [3], the mappings are required to satisfy Poisson's equations:

$$\begin{aligned} \alpha x_{\xi\xi} - 2\beta x_{\xi\eta} + \gamma x_{\eta\eta} &= -J^2 \left(P x_\xi + Q x_\eta\right) \alpha y_{\xi\xi} \\ & \quad -2\beta y_{\xi\eta} + \gamma y_{\eta\eta} \\ &= -J^2 \left(P y_\xi + Q y_\eta\right), \end{aligned} \tag{11}$$

$$\alpha = x_\eta^2 + y_\eta^2, \quad \beta = x_\xi x_\eta + y_\xi y_\eta, \quad \gamma = x_\xi^2 + x_\xi^2. \tag{12}$$

Using appropriate inhomogeneous terms P, Q in an iterative way, we may generate a grid point system in such a way that the spacial distribution of grid points is concentrated near the boundaries of the bodies and lines connecting adjacent grid points are orthogonal to the boundaries.

Finally, we stack up the grid points constructed on each 2D cross section in the direction of the axes of the cylinders and generate the aimed 3D grid point system in the computational domain. The constructed grid point system used for our numerical simulations is depicted in Figure 3. Figure 3(a) shows a general view of the whole grid point system by plotting grid points on the boundaries of the computational domain. Figure 3(b) gives a closeup of the grid points generated around the cylinders. The number of grid points in the direction of the flow (the direction of x-axis) is 239, that in the direction of the axes of the cylinders (the direction of z-axis) is 119 and that in the direction perpendicular to the x and z-axes (the direction of y-axis) is 91, and so the total number of the grid points is 2,588,131. In order to shorten the time for computation, we used a parallel computer of the distributed memory type. In the parallel computing, the whole computational domain is divided into subdomains as shown in Figure 3(c) and computation on each subdomain is allocated to each CPU. In the case of parallel computing of the distributed memory type, the allocated boundary data

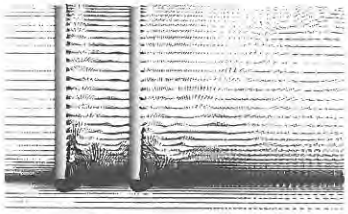

(a) Velocity vector

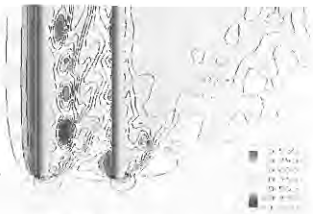

(b) Pressure contour

Fig 4 Computed results on x-z plane across circular cylinders

(a) Pressure

(b) Absolute vorticity

Fig 5 Computed iso-surfaces

are saved in separate memories. Hence we perform the parallel computing through the data communication using an MPI (Message Passing Interface) Library.

6 Results of Numerical Simulations

Computation is started with a uniform initial data and qualitative features are investigated by analyzing the numerical results of the simulation at a time step at which the flow field is well developed and reaches a quasi-stationary state. Figure 4 depicts the velocity vector field and contours of the pressure on the cross section containing the axes of the two cylinders. In the velocity vector field upward flows along the back of the front cylinder are observed. These upward flows are formed when the horizontal uniform flow runs around the bottom end and are remarkable in a neighborhood of the bottom end and even reach the top part of the cylinder. Similar upward flows are also observed behind the rear cylinder. These flows are formed in such a way that they seem to roll the bottom part up and go up towards the top part. Moreover, such upward flows are observed in a wide range behind the rear cylinder since there are no obstacles. In the figure of contours of the pressure it is observed that a vertical sequence of separate regions like cells of negative pressure are formed. This is due to the presence of nonstationary vorticities of Karmann-type.

On the other hand, a vertical sequence of regions of positive pressure are observed in the front of the rear cylinder. This phenomenon suggests that the nonstationary vorticities generated by the front cylinder interact the regions of stagnation existing in the front of the rear cylinder and deteriorate the stagnation pressure. Figure 5 depicts the iso-surfaces of pressure and vorticity and illustrates the 3D structure of the pressure field and vorticity distribution. It is observed in the pressure field that there is regular variation from the top part of the cylinders until the downstream due to the formation of vorticity pairs of Karmann type, and that in the bottom parts of the cylinders the variation of pressure is restricted to the rear sides.

On the other hand, concerning the vorticity distribution, regular variation due to the formation of vorticity pairs of Karmann type is observed in the top part of the rear cylinder in the same way as in the pressure field. Vorticity distribution is concentrated in the back of the middle part of the rear cylinder, although the vorticity distribution in the bottom part is comparatively sive. This suggests that the flows running around the bottom parts of the cylinders form longitudinal vortices. It is then inferred that these longitudinal vortices would motivate the upward flows behind the two cylinders. In Figure 6 the stream lines and trajectories of parti-

(a) streamline (b) Particle trajectory

Fig 6 Upward flow motion observed behind two circular cylinders

cles in the fluid are depicted. Trajectories of particles are drawn in the following way: We release the particles from the back of each cylinder and trace the trajectories forward and backward in time until the particles reach the boundaries of the computational domain and those of the bodies in the fluid. It is seen from Figure 6(a) that upward flows behind the cylinders are rolling up towards the top. Furthermore, the motion of longitudinal vortices around the bottom sides can be observed as inferred from the iso-surfaces of vorticities. Figure 6(b) is obtained by arranging particles on the same trajectories as in Figure 6(a) at regular time intervals. From this it is seen that the particle distribution represents how long a particle stay in the flow, and that particles are concentrated in the back of the front cylinder. These results of numerical simulations may have applications to various environmental problems. The farming part of an oyster raft as illustrated in Figure 1(a) may be regarded as a regular arrangement of cylinders with bottom ends. Our results suggests that red tide plankton would stay in the upward vortices rolling up along the back of the cylinders provided that the oyster raft is moved or water currents flow against the raft. Another application is that street trees as illustrated in Figure 1(b) are regarded as a sequence of cylinders with top ends, and that automobile exhaust fumes may be caught in the back of each tree which purify those poisonous gases. It is then expected that new environmental restoration technology will be developed by applying the results of numerical simulations for environmental fluids.

7 Concluding Remarks

New planning ideas of numerical simulations for environmental fluids have been obtained. By means of the simulation codes we have developed, we have performed numerical simulations of the flow fields around two cylinders with ends and have obtained the following results. Upward flows occur and roll up in the back of a cylinder. The flows are strong around the bottom end and get weaker towards the top end. Periodic sequences of vortices of Karmann type are remarkable in the upper parts of cylinders. In the case of two cylinders, periodically stable regions of low and high pressure between the front and rear cylinders. Around structures in environmental fluids, environmental disruptors are caught in the regions of low pressure behind the structures such as cylinders. In the case that two structures exist in an environmental fluid, environmental disruptors stay in between the structures and are transported as they move.

References

[1] E. Turkle, "Preconditioned Method for Solving the Incompressible and Low Speed Compressible Equations," *J. Comput. Phys.*, Vol.72, No. 2, pp.277–298, 1987

[2] T. Kawamura and K. Kuwahara, "Computation of High Reynolds Number Flow around a Circular Cylinder with Surface Roughness," AIAA Paper No. 84–0340, 1984.

[3] J. Thompson, Z. U. A. Warsi, and C. W. Mastin, "Numerical Grid Generation : Foundations and Applications," McGraw-Hill/Appleton & Lange, 1985

[4] H. N. Najm, P. S. Wyckoff, and O. M. Knio, "A Semi-implicit Numerical Scheme for Reacting Flow," *J. Comput. Phys.*, Vol.143, pp.381–402, 1998.